CHARACTERIZATION OF A PRE-VASCULARIZED BIOMIMETIC TISSUE ENGINEERED SCAFFOLD FOR BONE REGENERATION

By

JAMES A. CIPRIANO

A thesis submitted to the

School of Graduate Studies

Rutgers, The State University of New Jersey

In partial fulfillment of the requirements

For the degree of

Master of Science

Graduate Program in Biomedical Engineering

Written under the direction of

Dr. Joseph W. Freeman

And approved by

_____

_____

_____

New Brunswick, New Jersey

May 2018

ABSTRACT OF THE THESIS

Characterization of a Pre-Vascularized Biomimetic Tissue Engineered Scaffold for Bone Regeneration

By JAMES A. CIPRIANO

Thesis Director:

Dr. Joseph W. Freeman

Significant bone loss due to disease or severe injury can result in the need for a bone graft, with over 500,000 procedures occurring each year in the United States. However, the current standards for grafting, autografts and allografts, can result in increased patient morbidity or a high rate of failure respectively. An ideal alternative would be a biodegradable tissue engineered graft that fulfils the function of bone while promoting the growth of new bone tissue. We developed a pre-vascularized tissue engineered scaffold of electrospun biodegradable polymers PLLA and PDLA reinforced with hydroxyapatite, a mineral similar to that found in bone. A composite design was utilized to mimic the structure and function of human trabecular and cortical bone. These scaffolds were characterized mechanically and *in vitro* to determine osteoinductive and angioinductive properties. It was observed that further reinforcement is necessary for the scaffolds to mechanically match bone, but the scaffolds are successful at inducing the differentiation of mesenchymal stem cells into mature bone cells. Pre-vascularization was seen to have a positive effect on angiogenesis and cellular viability, critical factors for the integration of a graft.

ACKNOWLEDGEMENTS

I would like to thank Dr. Joseph Freeman for allowing me to study in his lab and guiding me over the course of three years. I am also very grateful for the people I've had the opportunity to work with in the MoTR lab. Dr. Brittany Taylor spearheaded this project before me and mentored me as an undergraduate. Mike Pellegrini has been a lifesaver on countless occasions, answering constant questions and cleaning up after my disaster hands. Adhithi Kanthan was an invaluable partner throughout almost every aspect of this study. Christian Buckley has taken up the future of the project, and it is in good hands with him. Dr. Daniel Browe, Pushpendra Patel, Xiomara Perez, Linh Mai, Het Patel, and Tiana Jayanathan have all helped me and contributed to the project in important ways as well. I'm sorry I can't list everybody but I also thank all past and present members of the lab who I haven't mentioned. Outside of the lab, I would like to thank Dr. Charles Gatt and Barbara Perry for their work on the animal study, Daniel Martin for imaging, and Lawrence Stromberg for making sure I had all the pieces in check. Lastly, but of course not least, I would like to thank my committee members Dr. Ronke Olabisi and Dr. Michael Dunn.

Equally as important are my friends and family who have supported me and kept me going. I'm incredibly lucky to have my parents for guidance, sisters for levity, and grandparents for encouragement, though to boil each down to one word is a terrible understatement. My girlfriend Veronica has been endlessly loving and supportive for over six years. I appreciate everybody in my life who has believed in me and am thankful for all of you.

TABLE OF CONTENTS

LIST OF FIGURES

LIST OF TABLES

CHAPTER 1- Introduction

1.1 Structure and Function of Bone

Bone is a hard tissue that serves as the body's foundation. It provides structure and shape, protects organs, and its joints define the way the body can move [1]. In addition to mechanical functions, bone also serves a metabolic function as a reservoir for minerals and blood cells [2]. The primary compositional components of bone are an organic collagen matrix and inorganic calcium phosphate nanocrystals. Calcium phosphate provides bone with its unique mechanical stiffness, or ability to resist deformation. Collagen, primarily type I, provides bone with viscoelasticity and mechanical toughness, or ability to absorb energy. Whole bone is comprised of approximately 65-70% inorganic material and 25-30% organic material [3].

Structurally, bone is comprised of two distinct types: cortical and trabecular. Cortical bone makes up the exterior of bone structures and provides mechanical strength, while trabecular bone is contained in the interior of the ends of long bones and contributes to shock absorption and marrow storage [4]. While both types consist of the same bone composition, the way in which the matrix is arranged results in vastly different mechanical properties. Cortical bone is highly structured and dense to maximize compressive strength, with an elastic modulus of 12-18 GPa and compressive strength of 130-180 MPa. Trabecular bone, also referred to as cancellous or spongy bone, is a porous meshwork of trabeculae innervated with blood vessels and bone marrow, with an elastic modulus of 0.1-0.5 GPa and compressive strength of 4-12 MPa [5]. Whole bone combines these two components to form an average elastic modulus of 1 GPa [6].

The basic functional unit of cortical bone is the osteon, a cylindrical formation of bone tissue surrounding a central blood vessel [7]. These rod-like units are formed by concentric layers of collagen known as lamella. The hollow center of the cylinder which houses a blood vessel is known as the Haversian canal, which branches into smaller lateral canals called Volksmann's canals. A visual representation of bone macrostructure and microstructure can be seen in the figure below.

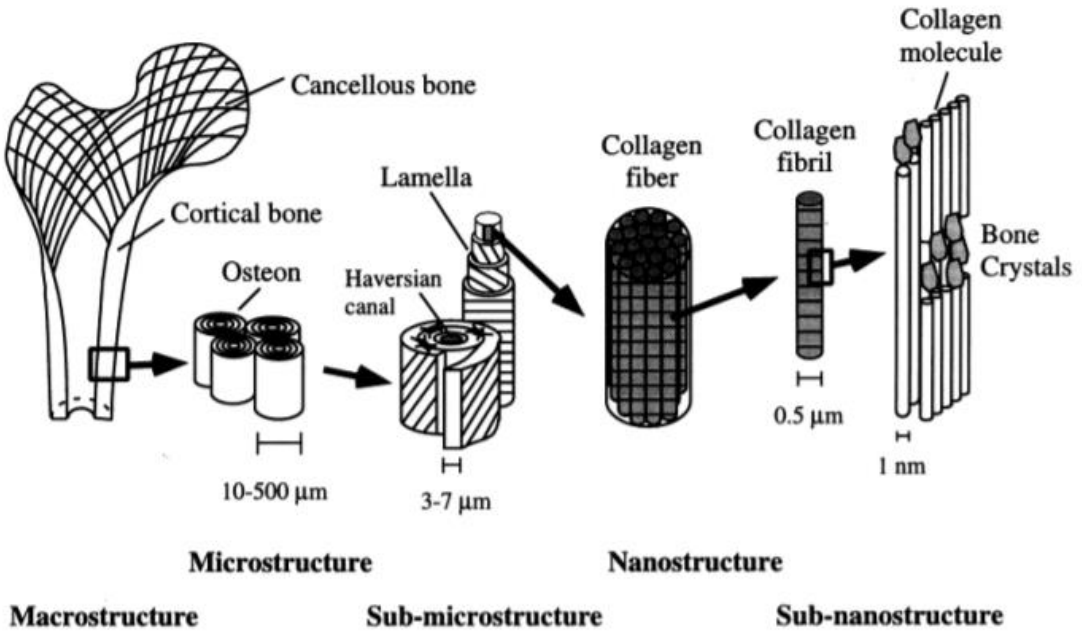

Figure 1: Hierarchical breakdown of bone structure [7].

1.2 Bone Injury and Healing

Bone is constantly remodeling itself through the action of osteoclasts and osteoblasts [8]. Osteoclasts are bone cells that resorb and break down existing bone matrix, which is then replaced by osteoblasts laying down new bone matrix. Remodeling is necessary for the

maintenance of healthy bone tissue, and an imbalance in the activity of osteoblasts and osteoclasts can result in conditions such as osteoporosis. In extreme cases of injury such as fractures, these remodeling tools are used to efficiently create new bone tissue and fuse existing bone structures [9].

Fractures can result from abnormal/extreme mechanical loading, fatigue from cyclic repeated loading, or normal loading on unhealthy or weakened bone [10]. Minor fractures are typically self-healing and need only a cast to secure the break in place and allow the bones to fuse together properly. In more severe cases, the fracture may need to be aligned with more invasive methods such as a bone plate[11]. However, in cases in which the bone loss is beyond that which the body is capable of repairing, either due to severe trauma exceeding critical size or bone disease affecting healing and remodeling facilities, a graft may be used to aid in repair. It is estimated that over 500,000 bone grafting procedures occur each year in the United States, and over 2 million worldwide[12].

1.3 Current Treatments

Grafting is a medical procedure defined by inserting existing tissue into a defect site that the body cannot repair on its own [13]. The treatment is commonly used to repair skin, bone, and ligaments. In the case of bone, the most desirable aspects of a graft are for it to be osteoconductive, osteoinductive, and osteogenetic [14]. Osteoconductive grafts are capable of serving as a scaffold for surrounding osteoblasts to migrate to and build new bone tissue upon. Osteoinduction refers to the ability of a graft to induce the differentiation of progenitor cells into osteoblasts, likely through the presence of growth

factors. Osteogenetic grafts contain their own osteoblasts and can independently generate new bone tissue without the presence of external cells. In addition to supporting osteoblast growth, grafts must also support the vascularization of new bone tissue [15].

Autografts are the current gold standard for bone grafting procedures [16]. They are defined by using bone tissue from the patient's own body as a graft. This tissue is typically harvested from the iliac crest of the pelvis. As they come from the body's own tissue, autografts are naturally osteoconductive and osteoinductive. In addition, they are the only graft capable of being osteogenetic because they contain native osteoblasts. However, autografts are an invasive procedure as they require a second surgery to harvest the grafting tissue [17]. This results in increased pain and morbidity for the patient when compared to other grafting options. Autograft supply is also limited by the amount of tissue that can be safely harvested from the patient. Patients with osteodegenerative conditions may not have the option of using autografts as well.

Allografts are made up of bone tissue that have been harvested from a donor cadaver [18]. These are the most commonly used grafts, making up one third of all bone grafting procedures in the United States, despite autografts being considered the gold standard [19]. Allografts are not limited by the disadvantages of limited supply and increased morbidity as autografts. However, they must undergo extensive sterilization procedures in order to mitigate an immune rejection upon implantation. Processing and sterilization have improved vastly in recent years, yet the integrity of the tissue must still be compromised when compared to autografts. This results in slightly less effective

osteoconduction and osteoinduction, as well as a lack of osteogenesis because foreign bone cells must be eliminated before implantation. Mechanical properties are also reduced up to 50% as a result of this processing. Long-term studies have found that allografts can have a failure rate up to 60% after ten years [6].

1.4 Bone Tissue Engineering

Tissue engineering is a concept that describes creating artificial grafts without requiring a donor or secondary surgery. These biodegradable grafts are designed to temporarily replace their target tissue while simultaneously inducing the growth of new healthy tissue as they are resorbed in the long term [20]. This is achieved by using the patient's own cells as a basis for growing tissue upon an implanted scaffold, with the addition of growth factors or other particles to enhance the cells' normal activity. Tissue engineered (TE) scaffolds should ideally match their target tissue in mechanical properties, be easily manufactured, biologically inert, conductive, inductive, and biodegradable over time [21]. These qualities would address the issues of morbidity and limited supply in autografts, as well as the lack of mechanical integrity and risk of infection in allografts.

Significant progress has been made in the field of tissue engineering for bone. Electrospun polymer scaffolds are of particular interest as they have been successful at producing environments favorable to osteoinduction [22]. This is achieved by dissolving a charged polymer in solution and extruding it from a syringe at a steady rate into an electric field. The polymer forms a thin fiber as it traverses the electric field, which can be collected on a spinning mandrel to create a sheet of aligned fibers. This process can be

visualized in the figure below. With proper adjustment of factors such as voltage, working distance, mandrel speed, and flow rate, the properties of the resulting scaffold can be predetermined.

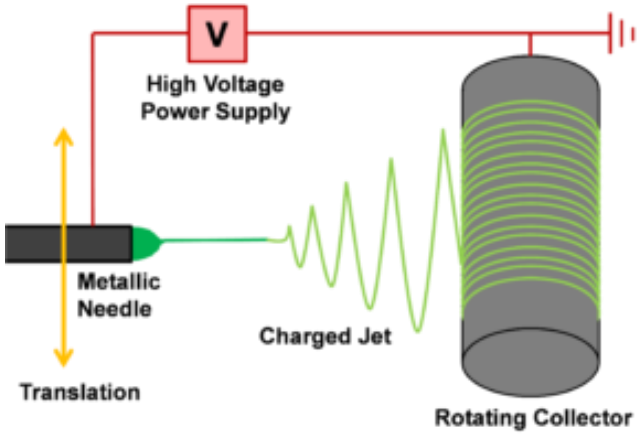

Figure 2: Schematic of the electrospinning setup [23].

Electrospun scaffolds with proper pore size can be used as osteoinductive environments, as osteoblasts tend to thrive in pores 5-200 μm [24]. Additional growth factors, mineral, or biological material can be included to increase osteogenic properties [25]. As such, polymer-based scaffolds are promising solutions to inducing bone growth. However, these scaffolds cannot achieve mechanical properties comparable to surrounding bone, and they can have difficulty becoming innervated with vasculature [26]. Ceramic-based scaffolds have been considered as well, which are able to achieve significantly greater mechanical properties [27]. Although this is an improvement over polymeric scaffolds, these scaffolds are less effective at integration with surrounding bone tissue and vasculature.

1.5 Aim of the Project

The aim of this project was to utilize previous designs of the MoTR lab to create a biomimetic scaffold with improved mechanical properties and vascular induction [28-33]. This scaffold consists of electrospun polymer constructed into both trabecular and cortical components with varying porosity and shape. The cortical components are designed to mimic the design of an osteon, with fibers oriented cylindrically about a central channel. Hydroxyapatite columns and mineralization are used to reinforce the mechanical properties, which are assessed via compression testing. The interior of the cortical channels are pre-vascularized with decellularized vascular matrix, while the rest of the scaffold is mineralized to improve osteoinduction. The ability of the scaffold to induce stem cell differentiation into both bone and endothelial cells was assessed *in vitro*.

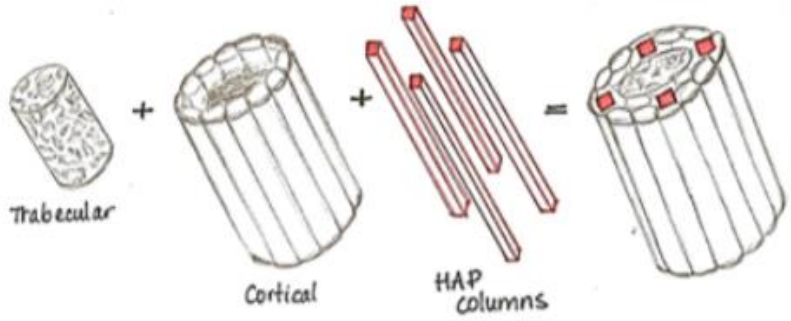

Figure 3: Schematic of complete scaffold and its components.

CHAPTER 2- Scaffold Fabrication and Characterization of Cellular Differentiation

The goal of this project was to analyze the mechanical and inductive properties of pre-vascularized bone-mimicking scaffolds. Complete scaffolds were created with electrospun polymer and sintered hydroxyapatite (HAp) columns, and their mechanical properties were determined through compressive testing. Simplified scaffolds of mineralized electrospun polymer were pre-vascularized with endothelial cells, decellularized, and seeded with human mesenchymal stem cells. Cell viability was tracked for both cell lines, and the differentiation of the stem cells was characterized by immunodetection of secreted proteins as well as cellular staining and imaging.

2.1 Materials and Methods

2.1.1 Fabrication of Electrospun Scaffolds

PDLA/PLLA Polymer Base

The primary components of the electrospun scaffolds are two forms of polylactic acid: poly-l-lactide (PLLA) and poly-d-lactide (PDLA). These biodegradable polymers have favorable mechanical properties for bone tissue engineering and are commonly used in such applications [22]. PLLA serves as the primary structural material, while PDLA serves as a sintering agent to solidify layers of PLLA adjacent to each other. To electrospin, a 7% (w/v) PLLA solution was prepared in solvents dichloromethane (DCM) and dimethylformaldehyde (DMF) with 10% gelatin. Gelatin was included to promote cellular proliferation by increasing the organic collagen content of the scaffold, as well as improve the mineralization of the scaffold by acting as a binding site for calcium phosphate [34]. PDLA was prepared at a concentration of 22% (w/v) in tetrahydrofuran

(THF) and DMF. PLLA (MW = 152,000) was purchased from Sigma Aldrich (St. Louis, MO, USA). PDLA (MW=124,000) was purchased from Evonik Birmingham Laboratories (Birmingham, AL, USA). Solvents DMC, DMF, and THF were purchased from Fisher Scientific (Pittsburgh, PA, USA).

Polymer solutions were loaded into a 5 mL syringe with an 18-gauge blunt needle and electrospun onto an 8 cm diameter aluminum mandrel rotating at approximately 2000 RPM. PLLA was spun at a working distance of 10 mm with voltage gradient +15kV/-10kV, while PDLA was spun at a working distance of 15 mm and voltage gradient +10kV/-5kV. PLLA/PDLA scaffolds were created by first spinning 1 mL of PDLA, followed by 5 mL of PDLA, and finally 1 mL of PDLA. This results in a sheet of PLLA with a thin layer of PLLA on either side, allowing the sheets to be layered and sintered upon each other into three-dimensional structures. For scaffolds intended for use in trabecular components, NaCl crystals were poured over the mandrel at a consistent rate as PLLA was electrospinning. These acted as porogens to be leached out at a later time.

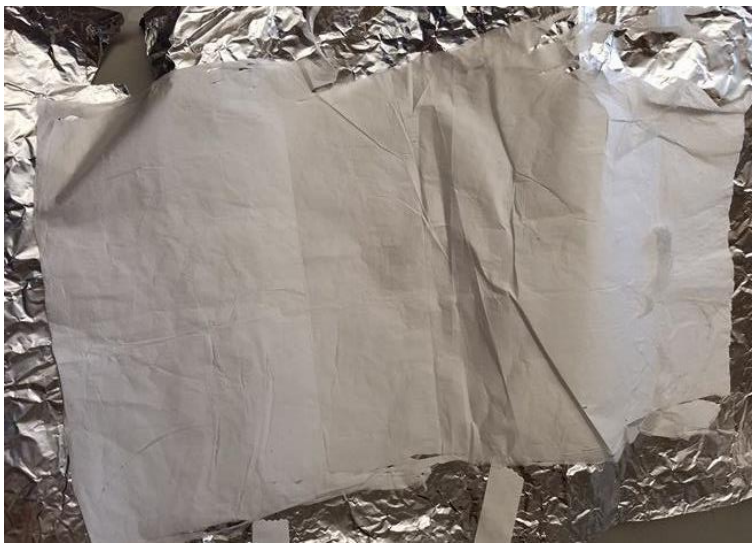

Figure 4: Electrospun sheet of PLLA/PDLA scaffold.

After being electrospun, scaffolds were stored in a desiccator to eliminate any remaining solvents.

Construction of Cortical Scaffold Components

Cortical scaffolds were created in the model of osteons, whereby PLLA/PDLA sheets were layered cylindrically about a hollow channel meant to evoke the Haversian canal. This effect was created by hand-wrapping a sheet of PLLA/PDLA scaffold about a mold created by a blunt 22 gauge needle, creating an inner diameter of 0.71 mm. The sheets were 2 cm wide in the circumferential direction and cut to their specific desired size in the lengthwise direction. The alignment was selected such that the fibers of the scaffold mimicked the 45˚ orientation of collagen fibers in the lamella of an osteon. In this study, scaffolds used for mechanical testing were cut to 6 mm of length, while scaffolds used for

cellular studies were cut to 3 mm of length. Once prepared on the molds, the scaffolds were sintered at 60˚C for 45 minutes.

To allow easy removal of the cortical scaffolds without damaging the inner layer of the channel, a thin layer of polyethylene oxide (PEO) was first wrapped about the mold. Electrospinning solution was made by dissolving 10% (w/v) PEO into 100% ethanol (EtOH) and deionized water (dI H_2O). PEO was purchased from Sigma Aldrich (St. Louis, MO, USA), and 100% ethanol (EtOH) was purchased from Fisher Scientific (Pittsburgh, PA, USA). PEO solution was then electrospun at a rate of 5 mL/hr with a working distance of 10 cm and voltage gradient of +10kV/-3kV. After the cortical scaffolds had been sintered, the PEO was leached in dI H_2O for 30 minutes and the remaining PLLA/PDLA scaffold was removed from the mold.

Construction of the Trabecular Scaffolds

Trabecular scaffolds were made using PLLA/PDLA sheets that had NaCl porogens included during the electrospinning process. Such sheets were cut into long 1.5 cm strips and wrapped upon themselves before being weighted and sintered at 60˚C for 45 minutes. Once solidified into compact rectangular shapes, the scaffolds were submerged in di H_2O for at least 3 hours to leach out the NaCl porogens. Resulting scaffolds were finally cut to size.

2.1.2 Fabrication of Hydroxyapatite Columns

Hydroxyapatite (HAp) columns were created using HAp nanopowder purchased from Sigma Aldrich. This powder was packed along with dI H_2O into a cylindrical mold of approximately 1.5 mm in diameter and 14 mm in depth. dI water was applied dropwise in regular intervals and acted to coagulate the powder into a solid column. Care was taken to ensure that an even amount of water was applied across the entire length of the column, for too little water would fail to solidify the powder while too much water would compromise the structural integrity as well as introduce micro cracks in the structure during the sintering process.

After being hand-packed into the mold, the columns were packed under 44 MPa of pressure by an Instron (Model 5869, Norwood MA) for 10 minutes. Upon removal from the mold, columns sintered for 5 hours at 1200˚C. Sintering was performed in a ThermoScientific EuroTherm 2116 Benchtop Muffle furnace. Once cooled, the columns were filed to the desired size using a Dremel.

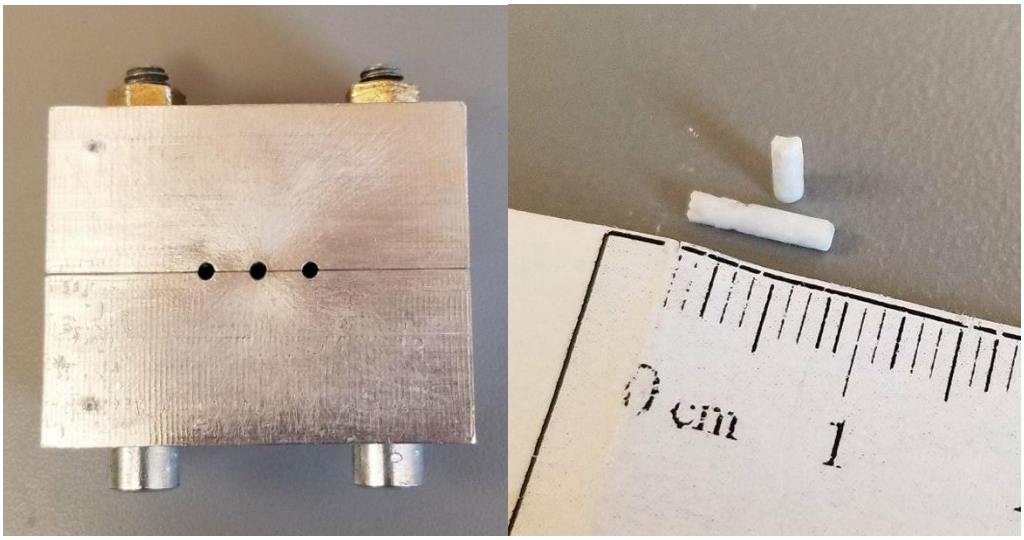

Figure 5: Left: Mold used for packing HAp columns. Right: Sintered HAp columns.

2.1.3 Scaffold Processing for Mechanical Testing

To prepare scaffolds for further use the polymer components must be gelatin crosslinked, constructed into complete scaffolds, and mineralized. Gelatin provides exposed carboxyl groups which act as binding sites for ions during mineralization, but must be crosslinked to retain its structure. Microbial transglutaminase (mTG) was chosen as the crosslinking agent based on previous studies. The cortical and trabecular scaffolds were submerged in 12% mTG in phosphate buffered saline (PBS) for five hours at 37˚C. After crosslinking, the scaffolds were washed with PBS three times to remove the mTG.

The individual cortical, trabecular, and hydroxyapatite components of the scaffold were combined into a complete scaffold for mechanical testing. Six cortical osteon channels and two hAP columns were arranged in a cylindrical shape about a rectangular trabecular

base. A strip of PDLA was wrapped about the entire structure and sintered for 45 minutes at 60˚C. PDLA application and sintering was repeated as necessary to ensure the components of the scaffold were bound into a complete whole.

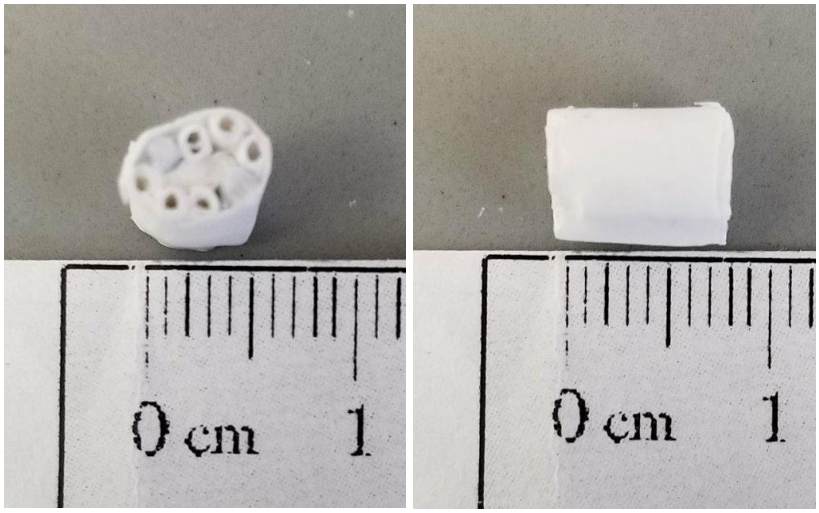

Figure 6: Top and side view of a complete scaffold.

Once the scaffolds were complete, the final processing step was mineralization to enhance the mechanical integrity of the structure as well as provide an environment to induce cellular differentiation down the osteogenic lineage. Static mineralization was performed by submerging the scaffolds in simulated body fluid (SBF) for 20 hours, with the SBF being changed every two hours. SBF was created with solutes sodium chloride (NaCl), potassium chloride (KCl), calcium chloride dihydrate ($CaCl•H_20$), magnesium chloride heptahydrate ($MgCl_2•H_20$), sodium bicarbonate (NaHCO3), and sodium phosphate monobasic (NaH_2PO_4) all dissolved in PBS. These solutes were purchased from Fisher Scientific (Pittsburgh, PA, USA).

2.1.4 Mechanical Testing

Sample size N=4 complete scaffolds were prepared for mechanical testing. To determine mechanical properties, the complete scaffolds were compressed at a strain rate of 10%, or extension of 0.6 mm/min, until failure. Compression was performed by an Instron 5869 system with a 50 kN load cell. Samples were kept dry and testing took place at room temperature. The load-extension data from the Instron was converted to stress-strain to determine the elastic modulus and ultimate compressive stress for each sample.

2.1.5 Scaffold Processing for *in Vitro* Study

Simplified versions of the complete scaffolds were prepared for *in vitro* testing. The purpose of this study was to track the differentiation of stem cells as they grew upon the scaffolds, specifically with respect to osteogenesis and angiogenesis. Three cortical channels were laid across a base of trabecular scaffold, and this structure was weighted and sintered. Hydroxyapatite columns were not included in these scaffolds because mechanical strength was not of interest for this study.

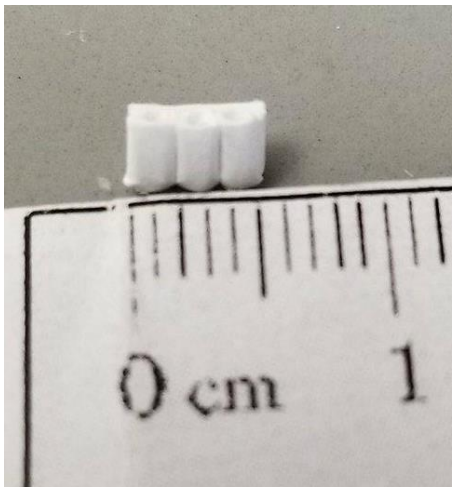

Figure 7: Simplified scaffold for in vitro study.

The simplified scaffolds were gelatin crosslinked as the complete scaffolds were in 12% mTG for five hours at 37˚C. Prior to mineralization, the three hollow channels of the cortical sections were filled with alginate, a hydrogel which has been shown to block mineralization [35]. This was done to create an environment more favorable for vascular cells within the channels rather than osteoblasts. 8% (w/v) alginate in PBS was used to fill the channels, and the hydrogel was polymerized in 0.1M calcium chloride ($CaCl_2$) in PBS. After the addition of alginate, the scaffolds were mineralized in SBF for 20 hours via static mineralization. To account for the lack of HAp columns in the scaffolds, separate HAp columns were included alongside the scaffolds in the SBF during mineralization to provide additional mineral content.

After mineralization, scaffolds were washed in PBS and warmed to 37˚C to soften the alginate, which was subsequently removed from the channels using a blunt needle.

Scaffolds were then sterilized in 70% ethanol (EtOH) for one hour and exposed to 30 minutes of UV on each side. Ethanol was washed away with sterile PBS and the scaffolds were pre-conditioned in HMEC-1 media at 37˚C overnight.

2.1.6 HMEC-1 Vascularization

Immortalized human microvascular endothelial cells (HMEC-1) and media were purchased from ATCC (CRL-3243). These cells were maintained and expanded in MDCDB-131 media supplemented with 10% FBS, 1% penicillin streptomycin, 10 mM L-Glutamine, 1 μg/mL hydrocortisone, and 0.1 ng/mL epidermal growth factor. Cells were housed in a humidified incubator at 37˚C and 5% CO_2, and media was changed every 2-3 days. Once confluency of approximately 80% was reached, the HMEC-1s were detached from their flask via TrypLE Express Reagent and seeded at P8 into the hollow cortical channels of the scaffolds at a density of 50,000 cells/cm^2 (3350 cells/channel). Cells were also applied to tissue culture plastic (TCP) at the same density to serve as a control, with sample size N=4. 24-well plates were used for both the samples and TCP controls.

HMEC-1 cells were grown on the samples for 14 days, with media changed on days 3, 7, 10, and 12. Metabolic activity, an indirect measure of cellular viability, was assessed using PrestoBlue® assay on days 3, 7, 10, and 14. For this process, PrestoBlue® reagent was applied in the dark to three representative scaffold wells on each plate, four TCP wells with HMEC-1 cells, and one blank well with no cells. After incubating for one

hour, the reagent was collected and transferred to a 96-well plate in triplicate. A Tecan M200 Microplate Reader was used to measure relative fluorescent absorbance at 570 nm. Relative fluorescence was obtained by subtracting the blank control and normalizing to cellular number.

2.1.7 Decellularization and hMSC Cell Seeding

After 14 days of vascularization, the HMEC-1 cells were eliminated from the scaffolds by a freeze-thaw decellularization process. The well plates were parafilmed and submerged in liquid nitrogen for ten minutes, then quickly transferred to warm 37˚C water for ten minutes. The samples were washed with PBS to remove cellular debris, and the freeze-thaw-wash cycle was performed a total of three times. This method was chosen to lyse and remove cells while maintaining the extracellular matrix and pro-angiogenic proteins that the vascular cells produced.

An *in vitro* study using human bone-marrow derived mesenchymal stem cells (hMSCs) was performed to determine the effect of pre-vascularization on cellular differentiation. hMSCs are known to differentiate into osteoblasts, chondrocytes, adiposites, and myoblasts depending on their environment [36]. It has also been observed that hMSCs can differentiate into endothelial cells *in vitro* [37, 38]. This study utilized three experimental groups: vascularized scaffolds (Group V), non-vascularized scaffolds (Group N), and TCP controls (TCP). Both groups of scaffolds had undergone gelatin crosslinking and mineralization, but only the samples of Group V had been seeded with

HMEC-1s and decellularized after 14 days. Sample size N=24 samples were prepared for each group. Prior to cell seeding, scaffolds were sterilized for 1 hour in EtOH and 30 minutes of UV on each side, and pre-conditioned overnight in hMSC media.

hMSCs were purchased from ATCC (PCS-500-012) and expanded in growth media for bone-marrow derived MSCs (ATCC PCS-500-041). This medium included 5 ng/mL rh FGF basic, 15 ng/mL rh IGF-1, 7% FBS, and 2.4 mM L-Alanyl L-Glutamine, and served to maintain the multipotent quality of the MSCs. At 80% confluency, the cells were removed from their flask by TripLE Express Reagent and seeded onto the scaffolds at a density of 30,000 cells/cm^2. Cells were applied into the cortical channels as well as on the surface of the trabecular section. The same cellular density per surface area was used for the TCP control wells. After seeding, the cellular media was changed from the hMSC growth medium to α-MEM supplemented with 10% FBS and 1% penicillin streptomycin. Ascorbic acid was not included in the α-MEM as exposure to ascorbic acid could push the stem cells down an osteogenic lineage. The purpose of this change in medium was to allow the hMSCs to differentiate based only on influences from the scaffolds they had been seeded on.

The hMSCs grew on the samples for 12 days, with media changed every 2-3 days. PrestoBlue® assay was used to observe metabolic activity on days 4, 7, and 12, and on each of these days media was saved for later analysis. N=8 samples were removed from each experimental group and fixed for imaging at time points 4, 8, and 12. A summary of

the experimental design can be seen in the table below. Vascular endothelial growth factor (VEGF), CD31, and VE-Cadherin were selected as angiogenic markers, and osteocalcin (OC) and alkaline phosphatase (ALP) were selected as osteogenic markers [39-42].

Day	Media Assays			Stains		
	PrestoBlue®	VEGF ELISA	Osteocalcin ELISA	CD31	VE-Cadherin	Alkaline Phosphatase
4	V=4 N=4 TCP=4	V=4 N=4 TCP=4	V=4 N=4 TCP=4	V=2 N=2	V=2 N=2	V=4 N=4 TCP=4
7	V=4 N=4 TCP=4	V=4 N=4 TCP=4	V=4 N=4 TCP=4	-	-	-
8	-	-	-	V=2 N=2	V=2 N=2	V=4 N=4 TCP=4
12	V=4 N=4 TCP=4	V=4 N=4 TCP=4	V=4 N=4 TCP=4	V=2 N=2	V=2 N=2	V=4 N=4 TCP=4

Table 1: Number of samples used for each assay at each time point from Group V (vascularized scaffolds), Group N (non-vascularized scaffolds), and TCP group (tissue culture plastic). All groups seeded with hMSCs.

2.1.8 Tracking Specific Marker Concentrations using ELISA

Enzyme-linked immunoabsorbant assay (ELISA) was performed to characterize the differentiation of the hMSCs throughout the 12-day study. Media collected at days 4, 7, and 12 were tested for VEGF, a common marker for angiogenesis and mature endothelial

cells, and osteocalcin, a marker known to characterize mature bone cells. The ELISA kits for VEGF and osteocalcin were purchased from RayBio® (ELH-VEGF and ELH-Osteocalcin, respectively). A dilution of 2x was used for VEGF, and 3x was used for OC.

2.1.9 Staining and Imaging

Sample size N=4 scaffolds and TCP wells were stained for alkaline phosphatase (ALP), an early marker for osteogenesis, at time points 4, 8, and 12. An ALP staining kit was purchased from Sigma Aldrich (86R Sigma) and used to fix and stain each sample. A Zeiss color microscope was used for imaging. The trabecular portion of the scaffold was targeted during imaging.

Sample size N=4 scaffolds and TCP wells were stained at time points 3, 8, and 12 for CD31 or VE-Cadherin, two integral membrane proteins used to identify endothelial cells. DAPI and phalloidin were included as well to identify cellular nuclei and actin, respectively. These samples were fixed in 3.7% paraformaldehyde for 10 minutes and sectioned into 40 μm slices. The sections were permeabilized in 0.5% Triton X-100 for 15 minutes, and blocked in 1% BSA for 30 minutes. CD31 or VE-Cadherin primary monoclonal antibody was applied at room temperature for one hour. A dilution of 1:75 used for CD31 antibody and a 1:333 dilution was used for VE-Cadherin antibody. Goat anti-Mouse IgG Alexa Fluor Plus 647 secondary antibody was applied for 1 hour at a dilution of 1:1000. Lastly, the samples were incubated for 20 minutes in DAPI and Phalloidin Alexa Fluor 488. PBS washes were included in between each of the staining

steps. Imaging was performed using a Zeiss confocal microscope. Antibodies were purchased from Thermo Fisher Scientific.

2.1.10 Statistical Analysis

All data was subjected to a one-way analysis of variance (ANOVA) with Tukey's post hoc test at a significance level of $p<0.05$. Statistical analysis was performed using KaleidaGraph Synergy Software.

2.2 Results

2.2.1 Mechanical Testing

Load-Extension data was collected from the Instron 5869 after compression testing of the complete scaffolds to failure. This data was converted to stress-strain based on the dimensions of the sample, and a representative stress-strain curve is displayed below. Elastic modulus was calculated as the slope of the longest linear region, yield stress was selected as the final point of that linear region, and ultimate compressive stress was determined by maximum stress on the curve. The results of these properties are as follows: Elastic modulus 272±183 MPa, yield stress 2.13±0.50 MPa, ultimate compressive stress 2.89±0.77 MPa.

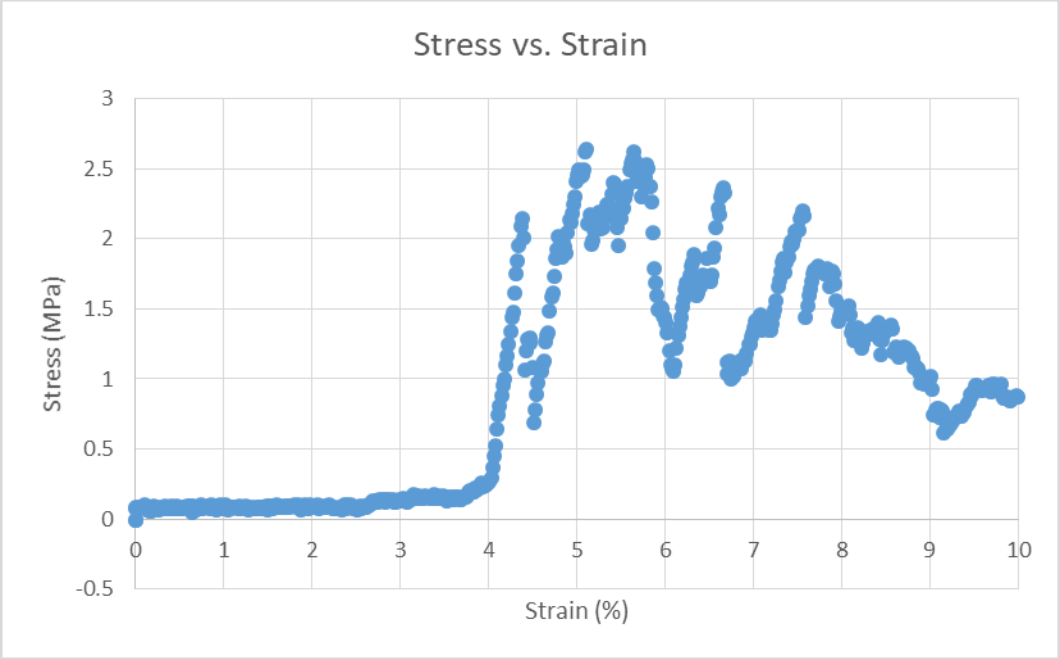

Figure 8: Sample stress vs. strain curve for a complete scaffold.

2.2.2 HMEC-1 Cellular Viability

Throughout HMEC-1 growth and vascularization upon the scaffolds, metabolic activity, an indirect measure of cellular viability, was assessed via PrestoBlue® assay on days 3, 7 and 14. Relative fluorescence units (RFU) obtained at 570 nm excitation were normalized by a blank media test as well as by cell number. There was a gradual increase in viability in both the scaffolds and the TCP group between days 3 and 14, though no viability changes were large enough to be considered significant.

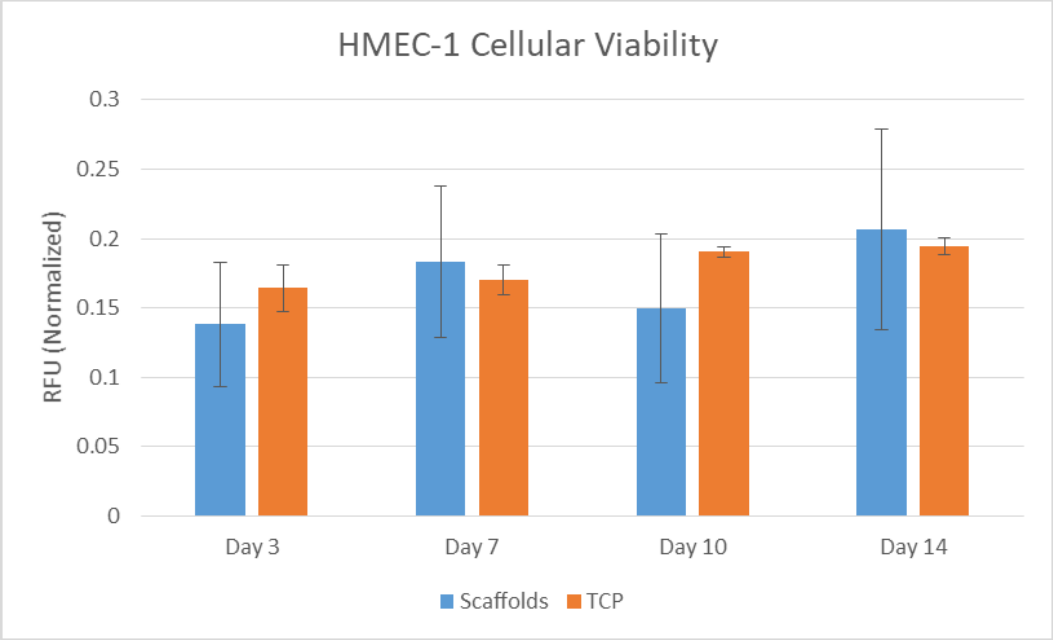

Figure 9: Cellular viability of HMEC-1 cells on scaffolds and TCP.

2.2.3 hMSC Cellular Viability

Cellular viability was assessed through the metabolic activity of hMSCs as they grew upon vascularized scaffolds (Group V), non-vascularized scaffolds (Group N), and TCP. PrestoBlue® assay was performed on days 4, 7, and 12 at an excitation of 570 nm. Relative fluorescence units (RFU) were normalized by blank media and cellular number. Cells on TCP had significantly greater viability than the cells on scaffolds, but remained relatively stagnant throughout the length of the study. Group V cells had greater viability than Group N cells, and while both groups experienced a significant increase in viability on day 12 the increase was greater for Group V.

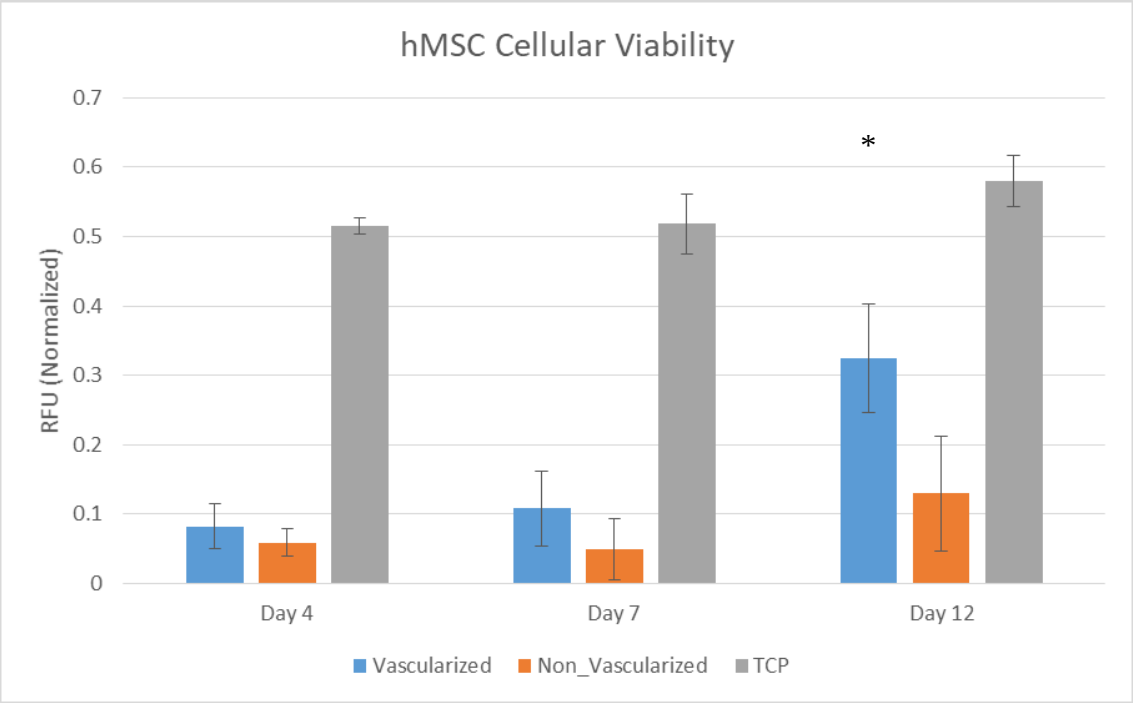

Figure 10: Cellular viability of hMSCs on vascularized scaffolds, non-vascularized scaffolds, and TCP. Statistical analysis: Statistical analysis: * denotes ANOVA Tukey Test (post-hoc) $p<0.05$ from other scaffold groups. All TCP groups are significantly greater than all scaffold groups.

2.2.4 Osteocalcin and VEGF ELISA

Osteocalcin (OC), an osteogenesis marker, and vascular endothelial growth factor (VEGF), an angiogenesis marker, were assessed by ELISA on days 4, 7, and 12 of hMSC growth. OC concentration (ng/mL) is displayed in the figure below. Results were normalized to cell number. Overall, there was little trend in any group over the course of the study, although the scaffold groups are all significantly greater than the TCP groups. A decrease was seen in the vascularized scaffolds at day 12.

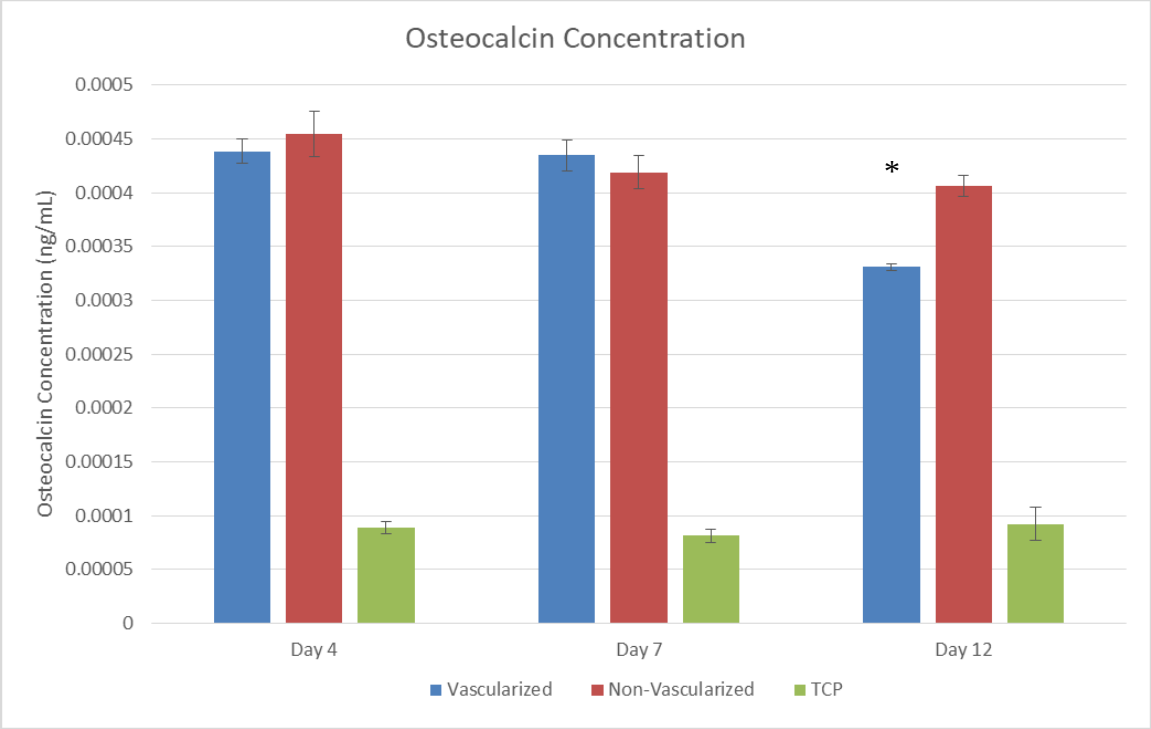

Figure 11: Osteocalcin ELISA results displaying concentration in vascularized, non-vascularized, and TCP groups seeded with hMSCs over time. Statistical analysis: * denotes ANOVA Tukey Test (post-hoc) $p<0.05$ from other scaffold groups. All scaffold groups are significantly greater than all TCP groups.

The VEGF ELISA results are displayed below for hMSCs. The TCP group contained significantly greater concentration of VEGF than the scaffold groups, and increased at each time point. Both Group V and Group N increased gradually at each time point, with a significant increase observed in Group V at day 12.

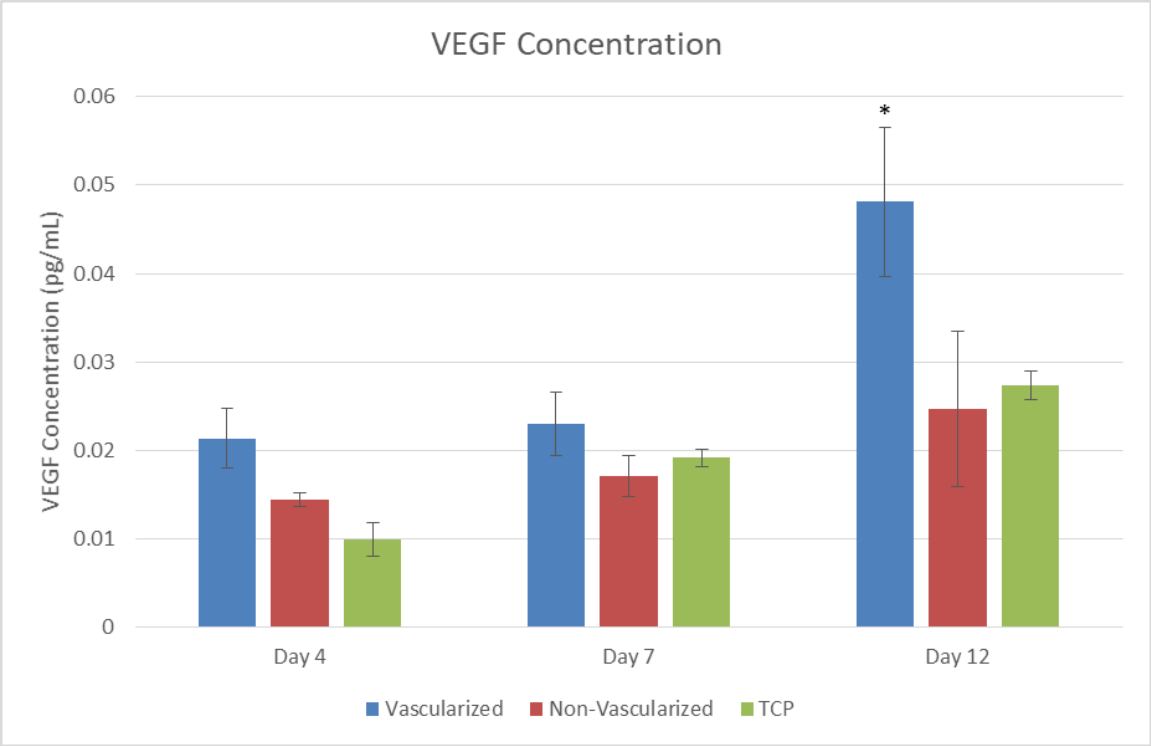

Figure 12: VEGF ELISA results displaying concentration in vascularized, non-vascularized, and TCP groups seeded with hMSCs over time. Statistical analysis: * denotes ANOVA Tukey Test (post-hoc) $p<0.05$ from all other groups.

2.2.5 Alkaline Phosphatase Imaging

Alkaline phosphatase (ALP), a protein expressed in the early stages of osteogenesis, was stained at days 4, 8, and 12 for vascularized scaffolds, non-vascularized scaffolds, and TCP. The blue color in the images below represents stained ALP protein. Stained protein was most abundant on the scaffolds at day 8. There was no clear difference in the presence of ALP on Group V and Group N scaffolds.

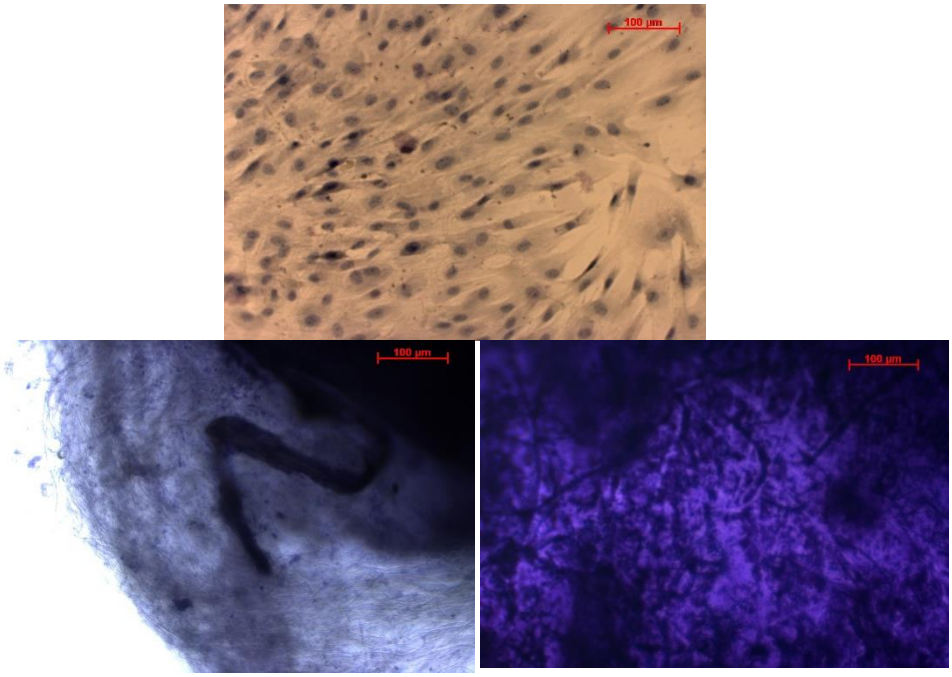

Figure 13: ALP stain of hMSCs at day 4. Top: TCP; Left: Non-Vascularized; Right: Vascularized. Images taken at 20x.

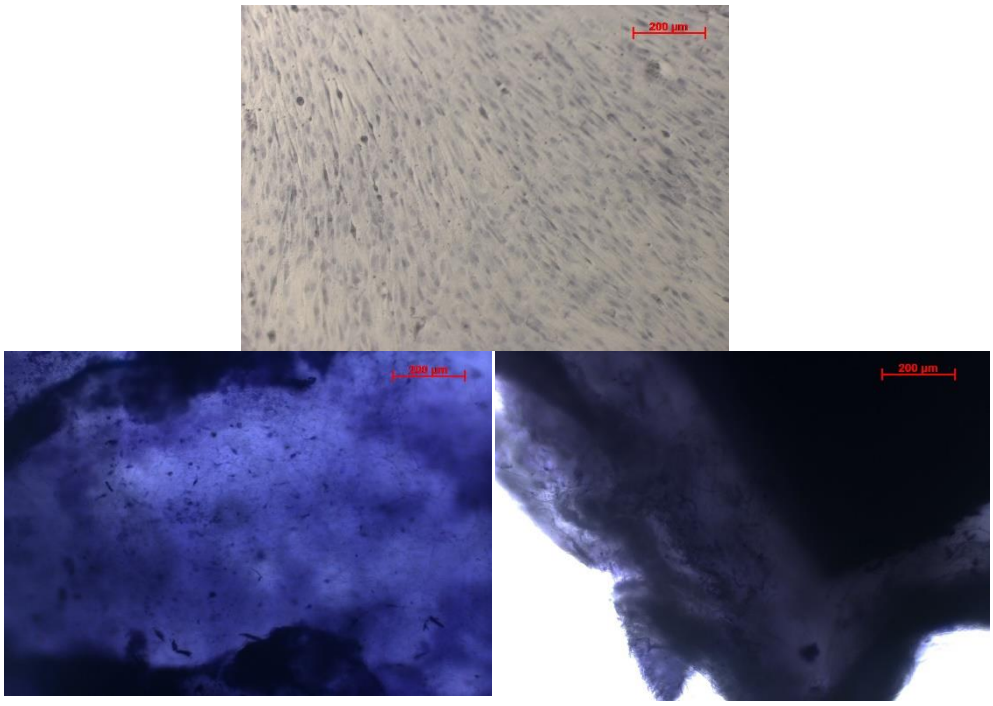

Figure 14: ALP stain of hMSCs at day 8. Top: TCP; Left: Non-Vascularized; Right: Vascularized. Images taken at 10x.

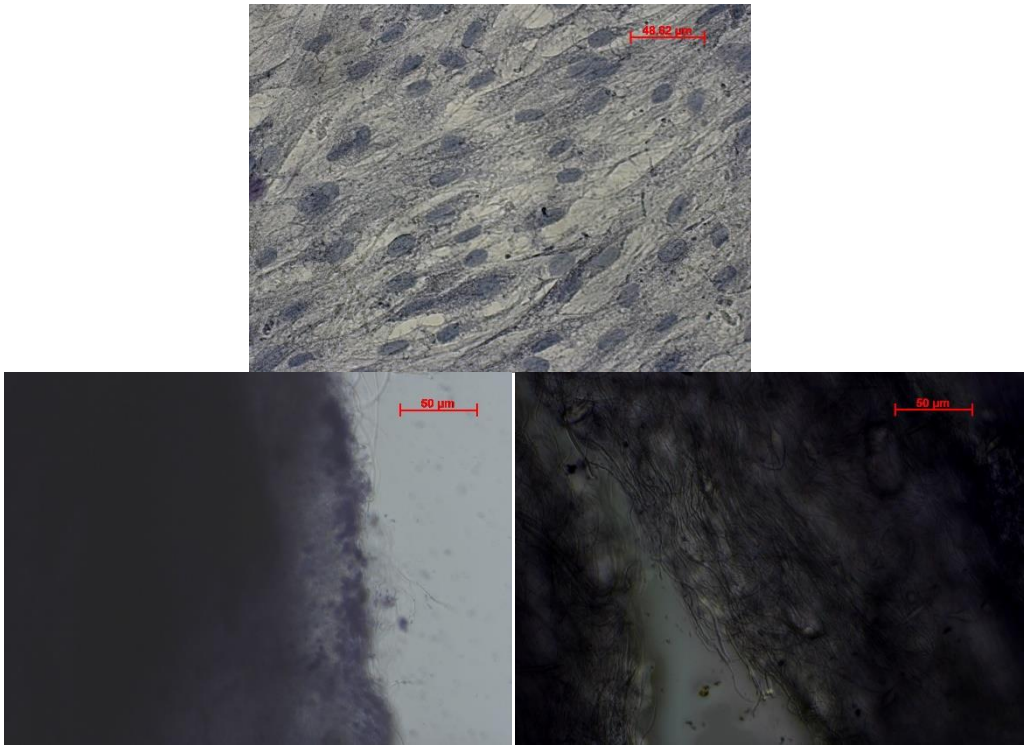

Figure 15: ALP stain of hMSCs at day 12. Top: TCP; Left: Non-Vascularized; Right: Vascularized. Images taken at 40x.

2.2.6 CD31 and VE-Cadherin Imaging

CD31 and VE-Cadherin, two membrane proteins unique to endothelial cells, were stained at days 4, 8, and 12 for vascularized scaffolds and non-vascularized scaffolds seeded with hMSCs. DAPI and phalloidin were stained as well to visualize cellular morphology. Scaffolds seeded with HMEC-1s were used as a positive control, and were stained for CD31, VE-Cadherin, and DAPI. In the images below, red represents either CD31 or VE-

Cadherin, blue represents DAPI, and green represents phalloidin. All images are taken at 10x and focused on the center of a cortical channel unless noted otherwise.

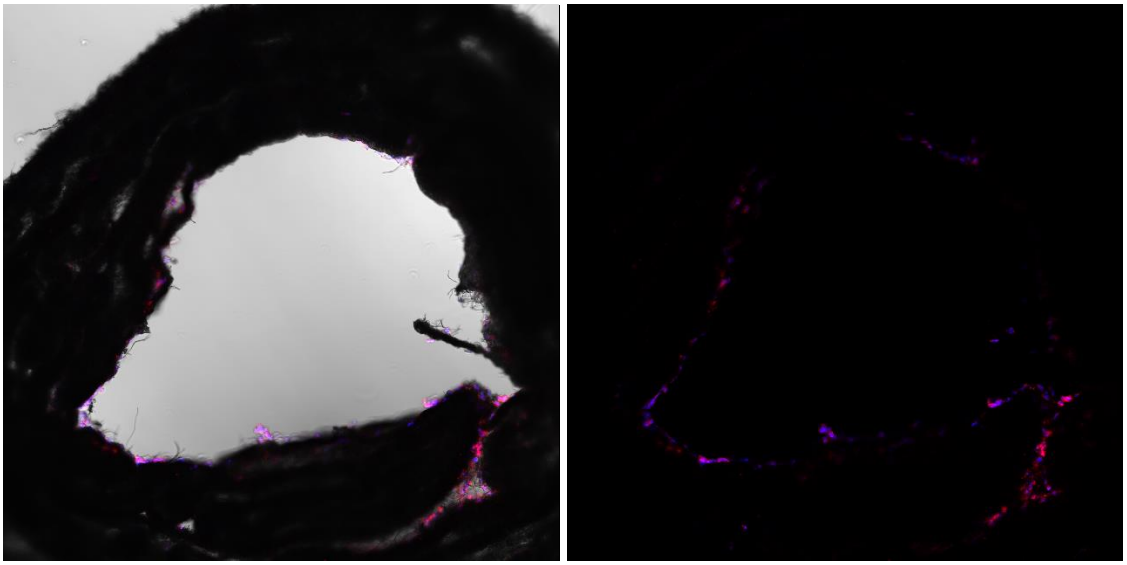

Figure 16: CD31 (red) and DAPI (blue) stained HMEC-1s at Day 14. Left includes visible image of scaffold, right is fluorescent image only.

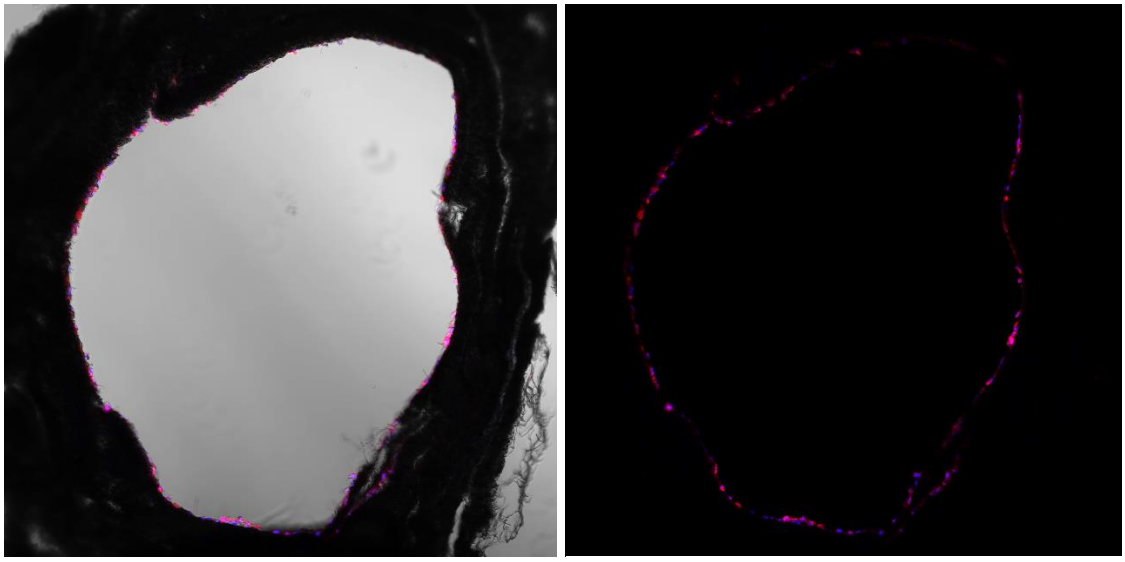

Figure 17: VE-Cadherin (red) and DAPI (blue) stained HMEC-1s at Day 14. Left includes visible image of scaffold, right is fluorescent image only.

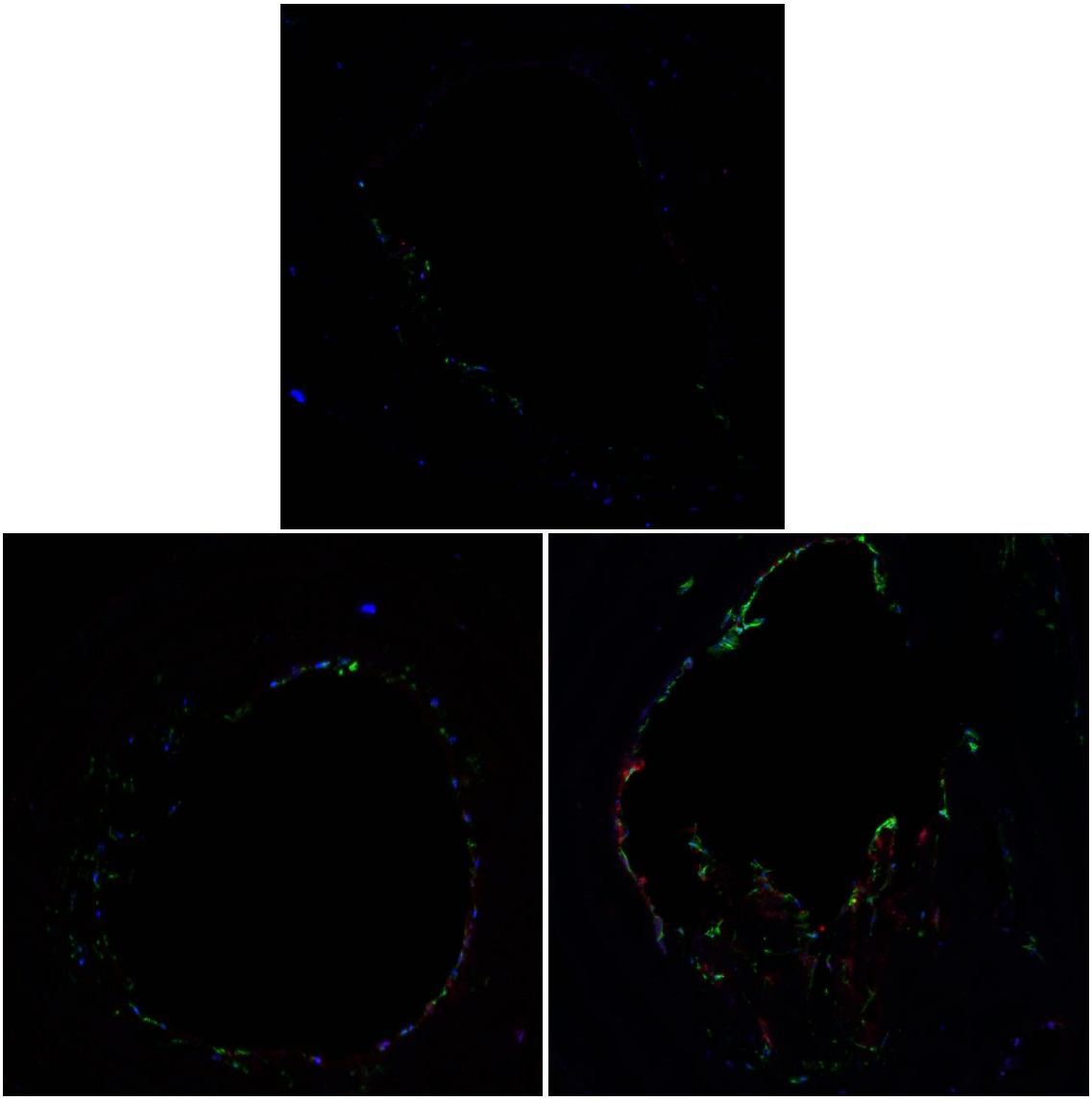

Figure 18: CD31 (red), DAPI (blue), and phalloidin (green) stained hMSCs at Day 4 (top), Day 8 (left), and Day 12 (right). Vascularized scaffolds.

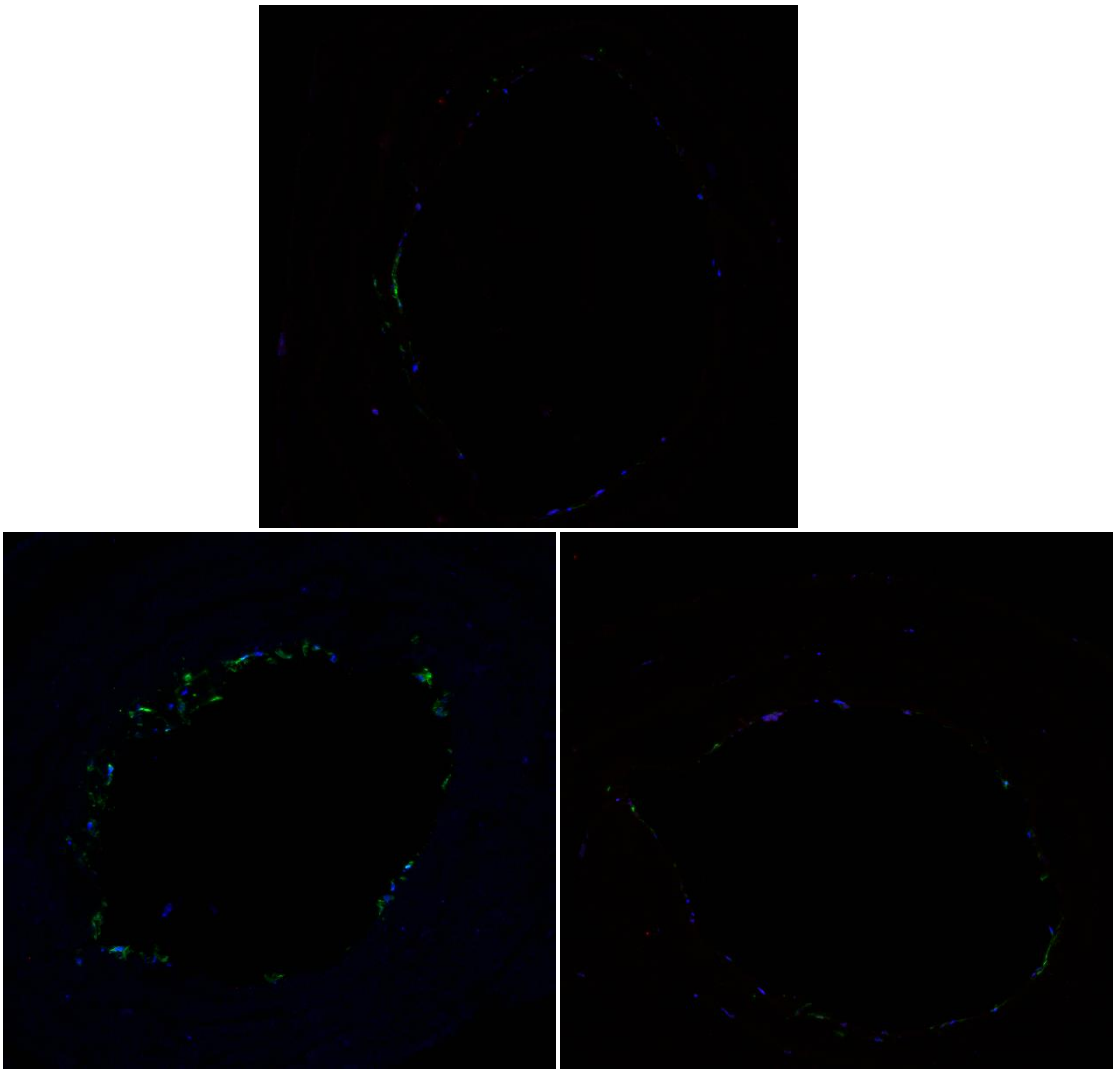

Figure 19: CD31 (red), DAPI (blue), and phalloidin (green) stained hMSCs at Day 4 (top), Day 8 (left), and Day 12 (right). Non-vascularized scaffolds.

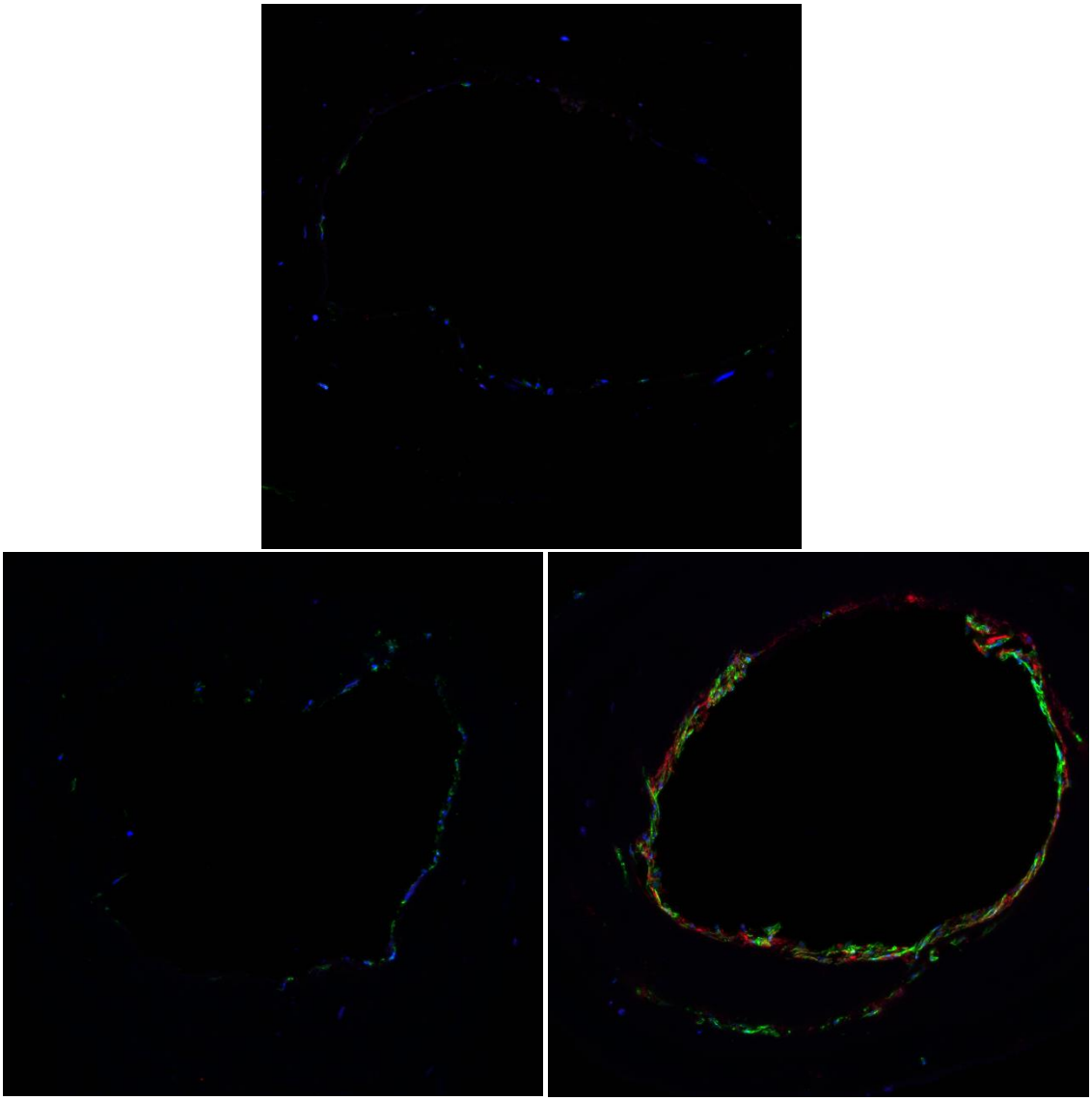

Figure 20: VE-Cadherin (red), DAPI (blue), and phalloidin (green) stained hMSCs at Day 4 (top), Day 8 (left), and Day 12 (right). Vascularized scaffolds.

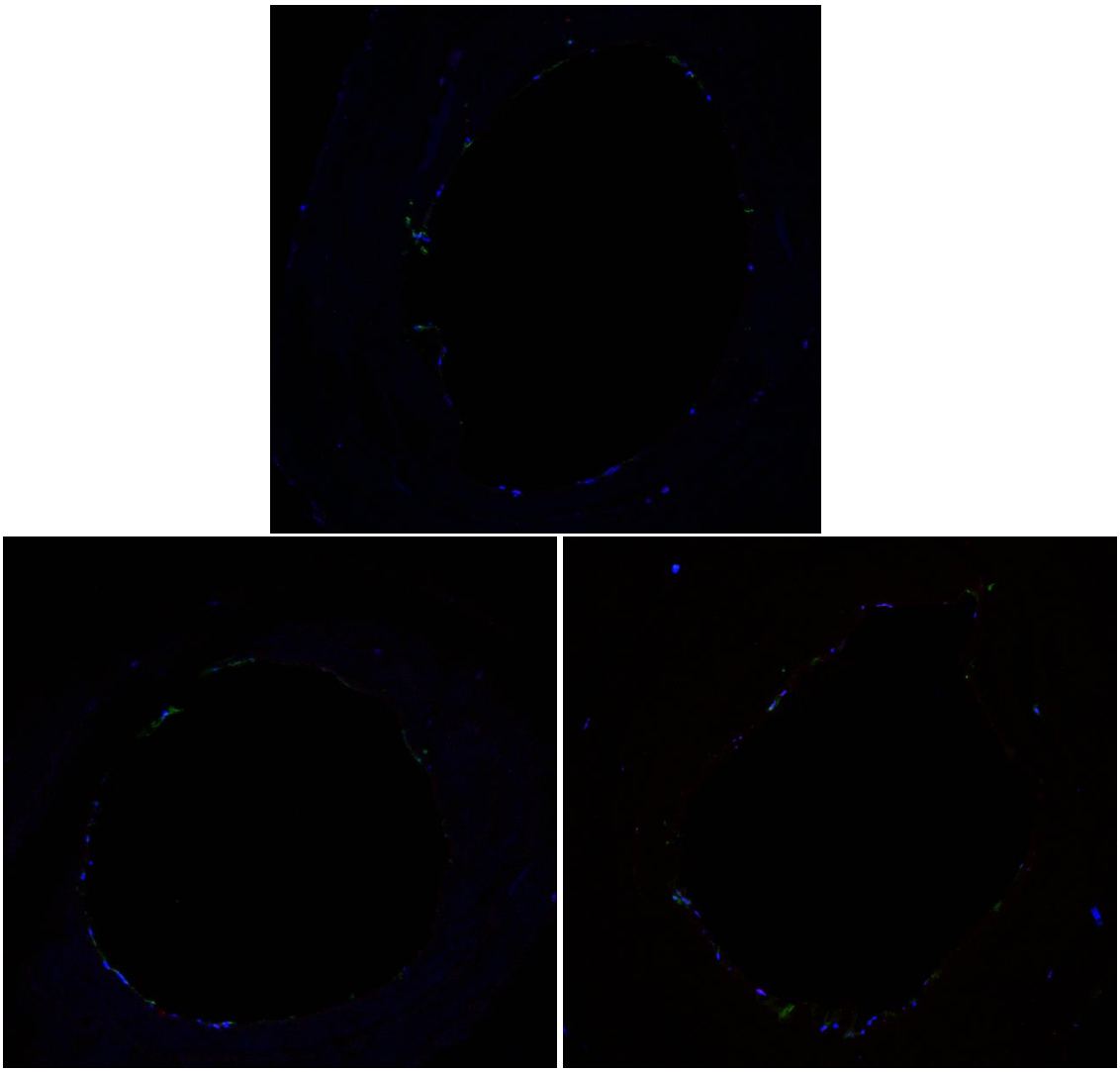

Figure 21: VE-Cadherin (red), DAPI (blue), and phalloidin (green) stained hMSCs at Day 4 (top), Day 8 (left), and Day 12 (right). Non-vascularized scaffolds.

From the images above, it can be seen that CD31 and VE-Cadherin were most abundant on vascularized scaffolds at day 12, reaching levels comparable to those found in HMEC-1 cells. To visualize cellular morphology, an image can be seen below of VE-Cadherin

stained hMSCs at day 12 on a vascularized scaffold. The actin can be seen conforming to the fibrous shape of the scaffold surface.

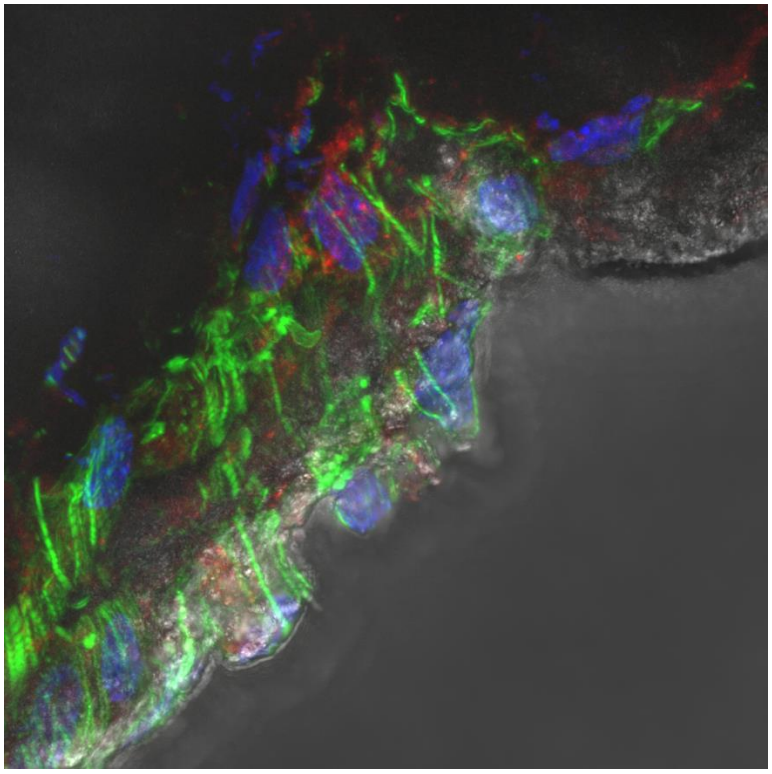

Figure 22: VE-Cadherin (red), DAPI (blue), and phalloidin (green) stained hMSCs at Day 12 on a vascularized scaffold. Image taken at 40x.

2.3 Discussion

The purpose of this project was to investigate the mechanical properties of a biomimetic scaffold and to determine the effect of pre-vascularization on the differentiation of mesenchymal stem cells into osteoblasts and endothelial cells. Complete scaffolds were used for mechanical testing, while cell differentiation was studied *in vitro* with simplified scaffolds. The base material was electrospun PLLA, PDLA, and crosslinked gelatin,

which had been shaped into a porous trabecular component and osteon-mimicking cortical components. Hydroxyapatite columns were included in the complete scaffolds for mechanical reinforcement. Both scaffolds were mineralized to improve mechanical properties and osteoinduction, but mineralization was blocked within the cortical channels of the simplified *in vitro* scaffolds to improve vascularization in that area.

The mechanical properties of the complete scaffolds were found to be approximately on par with trabecular bone, with a similar elastic modulus and low ultimate compressive stress. However, it is likely that early failure at a low compressive stress occurred due to the structure of the scaffold rather than the material itself. As the scaffold was handmade, the channels and posts had an inherent degree of misalignment with respect to the direction of compression. Thus as the scaffold was compressed, the angle continually increased resulting in little resistive force against the compression. This issue could be addressed by improving the bonds between the individual components of the scaffold using an adhesive such as fibrin glue. The outer layer of the scaffold could be reinforced as well, as only PDLA was used to hold the components together. Using PLLA/PDLA compound may improve the structural integrity of the scaffold. Increasing the time of mineralization is another variable to investigate. In addition, using a method such as 3D printing to increase reproducibility and post alignment would greatly improve mechanical properties.

Cellular viability for HMEC-1 cells was similar on both the scaffolds and the TCP, indicating that the scaffolds are a favorable environment for cellular growth. There was little growth between day 3 and day 14, indicating that the cells reached confluency within the first three days. This is consistent with results seen when growing HMEC-1 cells in tissue culture, as they have been observed to be a rapidly multiplying cell line. Cellular viability for hMSCs was significantly lower in the cells than the TCP, which is likely a consequence of the PrestoBlue® assay as a measure of metabolic activity. Metabolic activity was lower on the scaffold groups as the cells were differentiating, which can be confirmed by the osteocalcin ELISA results. Cells were also seen to be more viable on vascularized scaffolds than non-vascularized scaffolds, with Group V experiencing a significant increase in viability at day 12.

The osteocalcin ELISA results displayed that both vascularized and non-vascularized scaffold groups have significantly greater OC concentration than the TCP group. This indicates that the scaffold does have effective osteoinductive properties. Although the concentraions of OC are similar between Groups V and N at days 4 and 7, there is a significant decrease in OC concentration at day 12 for Group V. A longer study must be performed to observe if this trend will continue into further time points. However, there is little data to suggest that pre-vascularization has an adverse effect on osteoinduction.

The VEGF ELISA results displayed a clear trend as an increase was observed in all groups at each time point. The scaffold groups displayed a smaller concentration than the

TCP group, which is likely due to having fewer cells. Group V displayed greater VEGF concentration than Group N, with a significantly larger increase at day 12. This is an indication that pre-vascularization does have a positive effect on hMSC differentiation towards a vascular lineage.

Alkaline phosphatase stain was observed in both the TCP group and scaffold groups at all time points. Day 8 showed the greatest presence of ALP, which is consistent with the expected trend of ALP as an early osteogenic marker. The trabecular region was selected for imaging, as the cortical region of Group V is desired to be a site of angiogenesis. There was no significant difference between the two scaffold groups, indicating that vascularization of the cortical channels does not affect the osteoinduction of other areas of the scaffold.

CD31 and VE-Cadherin staining was used to highlight endothelial cells within the cortical channels. Although the markers could be identified in small amounts at other time points, the day 12 vascularized scaffolds displayed far greater stain than any other group. This indicates that significant cellular growth and angiogenesis occurred between days 8 and 12 in scaffolds of Group V. These results are consistent with those found by the PrestoBlue® assay and VEGF ELISA, where Group V experienced a spike in cellular viability and VEGF concentration at day 12 relative to Group N. Overall, there is strong evidence to suggest that pre-vascularization has a positive effect on cellular viability and angioinduction.

CHAPTER 3: Conclusion and Future Work

A biomimetic tissue engineered bone scaffold has been characterized mechanically and *in vitro* for inductive properties. The mechanical properties were found to be below that of bone, but can be improved with more effective binding of the scaffold components and improving fabrication techniques. Bone marrow-derived mesenchymal stem cells were observed to show signs of osteogenesis upon the scaffolds. Pre-vascularization of osteon-mimicking channels was effective at improving angiogenic induction, a characteristic which is essential for graft integration. A composite tissue engineered approach continues to be a promising alternative to current bone grafting options.

Studies are ongoing to continue characterizing and improving these scaffolds. They are being tested *in vivo* as a radial defect graft in rabbits. At the time of writing, two subjects were implanted with the graft and had no signs of rejection after eight weeks. The arm is functional and weight-bearing with a cast. Furthermore, alternate approaches are being explored to improve the efficiency of creating the scaffolds. 3D printed PLA scaffolds have been developed and are being studied alongside the electrospun scaffolds, and methods are being investigated to 3D print hydroxyapatite as well.

REFERENCES

1. Hing, K.A., *Bone repair in the twenty–first century: biology, chemistry or engineering?* Philosophical Transactions of the Royal Society of London. Series A: Mathematical, Physical and Engineering Sciences, 2004. **362**(1825): p. 2821-2850.
2. Weiner, S., W. Traub, and H.D. Wagner, *Lamellar Bone: Structure–Function Relations.* Journal of Structural Biology, 1999. **126**(3): p. 241-255.
3. Boskey, A.L., *Bone composition: relationship to bone fragility and antiosteoporotic drug effects.* BoneKEy Rep, 2013. **2**.
4. Keaveny, T.M., et al., *BIOMECHANICS OF TRABECULAR BONE.* Annual Review of Biomedical Engineering, 2001. **3**(1): p. 307.
5. Rezwan, K., et al., *Biodegradable and bioactive porous polymer/inorganic composite scaffolds for bone tissue engineering.* Biomaterials, 2006. **27**(18): p. 3413-3431.
6. Wheeler, D.L. and W.F. Enneking, *Allograft bone decreases in strength in vivo over time.* Clinical Orthopaedics and Related Research, 2005(435): p. 36-42.
7. Rho, J.Y., L. Kuhn-Spearing, and P. Zioupos, *Mechanical properties and the hierarchical structure of bone.* Medical Engineering and Physics, 1998. **20**(2): p. 92-102.
8. Christen, P., et al., *Least-detectable and age-related local in vivo bone remodelling assessed by time-lapse HR-pQCT.* PLoS ONE, 2018. **13**(1): p. 1-11.
9. Fillingham, Y. and J. Jacobs, *Bone grafts and their substitutes.* Bone Joint J, 2016. **98-b**(1 Suppl A): p. 6-9.
10. Hernandez, C.J., *Bone fatigue, stress fractures and bone repair (Sun Valley 2013).* IBMS BoneKEy, 2013. **10**.
11. Bray, R.S., *Bone plate stabilization system and method for its use*. 2006, Google Patents.
12. Campana, V., et al., *Bone substitutes in orthopaedic surgery: from basic science to clinical practice.* Journal of Materials Science. Materials in Medicine, 2014. **25**(10): p. 2445-2461.
13. Bose, S., M. Roy, and A. Bandyopadhyay, *Recent advances in bone tissue engineering scaffolds.* Trends in biotechnology, 2012. **30**(10): p. 546-554.
14. Henkel, J., et al., *Bone Regeneration Based on Tissue Engineering Conceptions-A 21st Century Perspective.* Bone Research, 2013. **1**: p. 216-248.
15. Oliver Cassell, C.S., et al., *Vascularisation of tissue-engineered grafts: the regulation of angiogenesis in reconstructive surgery and in disease states.* British Journal of Plastic Surgery, 2002. **55**(8): p. 603-610.
16. Sasso, R.C., et al., *Iliac Crest Bone Graft Donor Site Pain After Anterior Lumbar Interbody Fusion: A Prospective Patient Satisfaction Outcome Assessment.* Clinical Spine Surgery, 2005. **18**: p. S77-S81.
17. Brydone, A.S., D. Meek, and S. MacLaine, *Bone grafting, orthopaedic biomaterials, and the clinical need for bone engineering.* Proceedings of the Institution of Mechanical Engineers, Part H: Journal of Engineering in Medicine, 2010. **224**(12): p. 1329-1343.

18. Singh, A.K., et al., *Cross-correlative 3D micro-structural investigation of human bone processed into bone allografts.* Materials Science & Engineering C, 2016. **62**: p. 574-584.
19. Kinaci, A., V. Neuhaus, and D.C. Ring, *Trends in bone graft use in the United States.* Orthopedics, 2014. **37**(9): p. e783-8.
20. Dvir, T., et al., *Nanotechnological strategies for engineering complex tissues.* Nat Nanotechnol, 2011. **6**(1): p. 13-22.
21. O'Brien, F.J., *Biomaterials & scaffolds for tissue engineering.* Materials Today, 2011. **14**(3): p. 88-95.
22. Rezvani, Z., et al., *A bird's eye view on the use of electrospun nanofibrous scaffolds for bone tissue engineering: Current state-of-the-art, emerging directions and future trends.* Nanomedicine: Nanotechnology, Biology, and Medicine, 2016. **12**(7): p. 2181-2200.
23. *The electrospinning process*. 2017, NEI Corporation: Exploring the Capabilities of Electrospinning.
24. Sethuraman, S., U.M. Krishnan, and A. Subramanian, *Biomaterials and Nanotechnology for Tissue Engineering*. 2016: CRC Press. 78.
25. Brown, B.N. and S.F. Badylak, *Extracellular matrix as an inductive scaffold for functional tissue reconstruction.* Translational Research: The Journal of Laboratory & Clinical Medicine, 2014. **163**(4): p. 268.
26. Novosel, E.C., C. Kleinhans, and P.J. Kluger, *Vascularization is the key challenge in tissue engineering.* Advanced Drug Delivery Reviews, 2011. **63**(4): p. 300-311.
27. Moore, W.R., S.E. Graves, and G.I. Bain, *Synthetic bone graft substitutes.* ANZ J Surg, 2001. **71**(6): p. 354-61.
28. Taylor, B.L., *The development and characterization of an osteoinductive pre-vascularized scaffold for bone tissue regeneration.* 2016, Rutgers University: New Brunswick, NJ.
29. Andric, T., et al., *Fabrication and Characterization of Three-Dimensional Electrospun Scaffolds for Bone Tissue Engineering.* Regenerative Engineering and Translational Medicine, 2015. **1**(1): p. 32-41.
30. Andric, T., L.D. Wright, and J.W. Freeman, *Rapid Mineralization of Electrospun Scaffolds for Bone Tissue Engineering.* Journal of Biomaterials Science -- Polymer Edition, 2011. **22**(11): p. 1535-1550.
31. Taylor, B.L., et al., *Investigating processing techniques for bovine gelatin electrospun scaffolds for bone tissue regeneration.* J Biomed Mater Res B Appl Biomater, 2017. **105**(5): p. 1131-1140.
32. Andric, T., A.C. Sampson, and J.W. Freeman, *Fabrication and characterization of electrospun osteon mimicking scaffolds for bone tissue engineering.* Materials Science and Engineering: C, 2011. **31**(1): p. 2-8.
33. Wright, L.D., et al., *Fabrication and mechanical characterization of 3D electrospun scaffolds for tissue engineering.* Biomed Mater, 2010. **5**(5): p. 055006.
34. Choi, M.O. and Y.-J. Kim, *Fabrication of gelatin/calcium phosphate composite nanofibrous membranes by biomimetic mineralization.* International Journal of Biological Macromolecules, 2012. **50**(5): p. 1188-1194.

35. Yamamoto, K., et al., *Inhibitory Activity of Alginates against the Formation of Calcium Phosphate.* Bioscience, Biotechnology, and Biochemistry, 1992. **56**(1): p. 90-93.
36. Prockop, D.J., *Marrow Stromal Cells as Stem Cells for Nonhematopoietic Tissues.* Science, 1997. **276**(5309): p. 71-74.
37. Oswald, J., et al., *Mesenchymal Stem Cells Can Be Differentiated Into Endothelial Cells In Vitro.* STEM CELLS, 2004. **22**(3): p. 377-384.
38. Scherberich, A., et al., *Three-dimensional perfusion culture of human adipose tissue-derived endothelial and osteoblastic progenitors generates osteogenic constructs with intrinsic vascularization capacity.* Stem Cells, 2007. **25**(7): p. 1823-1829.
39. Kim, S.-S., et al., *Poly (lactide-co-glycolide)/hydroxyapatite composite scaffolds for bone tissue engineering.* Biomaterials, 2006. **27**(8): p. 1399-1409.
40. Stucki, U., et al., *Temporal and local appearance of alkaline phosphatase activity in early stages of guided bone regeneration.* Clinical Oral Implants Research, 2002. **12**(2): p. 121-127.
41. Fathi, F., et al., *Early-stage detection of VE-cadherin during endothelial differentiation of human mesenchymal stem cells using SPR biosensor.* Biosensors and Bioelectronics, 2017. **96**: p. 358-366.
42. Sabry, D., O. Noh, and M. Samir, *Comparative Evaluation for Potential Differentiation of Endothelial Progenitor Cells and Mesenchymal Stem Cells into Endothelial-Like Cells.* International Journal of Stem Cells, 2016. **9**(1): p. 44-52.